Hydrodynamic Effects of Static Liquid Height in the Thermolysis Reactor for Cu-Cl Cycle Hydrogen Production

M. W. Abdulrahman[1], N. Nassar[1]
[1]Rochester Institute of Technology (RIT), Department of Mechanical and Industrial Engineering
Dubai Silicon Oasis, Dubai, UAE
mwacad@rit.edu; nin8507@g.rit.edu

Abstract - *This investigation explicitly investigates the impact of static liquid height on the hydrodynamics of the thermolysis reactor in the copper chlorine cycle for hydrogen production. The gas holdup behaviour at a range of static liquid heights, from 45 to 65 m, was investigated in the paper using a 3D computational fluid dynamics (CFD) model. The model precisely represents the trend of gas holdup, as confirmed by experimental data and compared to a two-dimensional counterpart. The gas holdup decreases as the static liquid height increases, as evidenced by the maximal error of 48.6%. Critical insights into the reactor's performance and improved approaches to hydrogen production are provided by the three-dimensional model.*

Keywords**:** Static liquid height, 3D CFD, Gas holdup, Hydrogen production, Cu-Cl cycle.

1. Introduction

Hydrogen is necessary to sustainable energy solutions due to its ability to advance the transition to more environmentally friendly energy systems. It is essential for the mitigation of climate change due to its capacity to decrease greenhouse gas emissions. The production of hydrogen through thermochemical cycles is a novel approach. By employing nuclear reactors, these cycles can decompose water through a variety of chemical reactions. The copper-chlorine (CuCl) cycle, which was discovered at Argonne National Laboratories (ANL), is extremely efficient, even at low temperatures [1,2]. The CuCl cycle operates at elevated temperatures and generates heat through the use of oxygen. Many methods have been employed by scientists to ensure the efficient transfer of heat in the oxygen reactor. Studies have demonstrated that molten CuCl is effectively heated through direct contact heat transfer (DCHT), which entails the return of 600°C oxygen gas into the reactor [3,4]. This approach enhances reactor efficiency and employs oxygen gas as a thermal medium. Slurry bubble column reactors (SBCRs) facilitate the production of oxygen in the CuCl cycle. The interactions between gas, liquid, and solid are simplified by these multiphase reactors. The sparger-injected gas causes the reactor bed to bubble. The temperature of SBCR can be precisely regulated as a result of the specific heat of liquid. This causes them commercially adaptable. The scaling of SBCRs necessitates an understanding of kinetics, hydrodynamics, heat and mass transport, and other relevant factors. An essential SBCR performance indicator is the gas holdup, which denotes the reactor's gas volume fraction. Careful management of these factors is necessary for the design and operation of SBCRs in industry. The literature consolidates the results of the studies, emphasizing the importance of novel methodologies, experimental investigations, and CFD analyses in the context of reactor design and operation.

The scale-up of these systems was investigated by Abdulrahman [3-12] in terms of material and thermal balances. His research has improved heat transmission

and minimized thermal resistance by incorporating spiral baffled jackets, helical internal tubes, and half-pipe jackets into continuous stirred tank reactors (CSTRs). Abdulrahman's research focuses on the utilization of nuclear reactors as heat sources, with a particular emphasis on the CANDU Super Critical Water Reactor (SCWR) and the High Temperature Gas Reactor. His research indicated that the CANDU-SCWR required increased heat transfer rates to enhance process efficiency. In 2018, Abdulrahman suggested that the reactor be heated, and oxygen gas be reintroduced directly into it to optimize thermolysis [4]. Abdulrahman [5] conducted research on chemical reactors that are compatible with thermolysis for the purpose of producing oxygen. He maintains that the bubble column reactor is the optimal choice. The use of molten CuCl and O_2 gas in thermolysis reactor thermal hydraulics experiments presents a multitude of challenges. Abdulrahman [13-14] identified substitute materials through dimensional analysis in order to replicate the thermal hydraulic properties of the original substances. These cost-effective and accessible alternatives render experimentation more secure and enjoyable. Abdulrahman conducted experimental research on the thermal hydraulics of SBCR [4,15-16]. The investigation investigated the impact of superficial gas velocity (U_{gs}) and static liquid height (H) on the gas holdup (α_g), volumetric heat transfer coefficient (U_V), and liquid temperature of the bubble column reactor. Empirical equations were employed to express these effects. Experiments demonstrate that an increase in U_{gs} results in an increase in U_V, liquid temperature, and α_g. The transition velocity of SBCR was experimentally measured by Abdulrahman [17]. Experiments have demonstrated that the transition velocity between homogeneous and churn turbulent flow regimes decreases as H increases. In the industrial SBCRs, no slug flow regime was observed. Abdulrahman and Nassar [18] conducted a review of Eulerian CFD for the purposes of BCR and SBCR analysis. They assessed research that altered reactor design, superficial gas velocity, pressure, and solid concentration to investigate their impact on thermal hydraulics. The Eulerian CFD model accurately anticipates the performance of BCR and SBCR, according to the review.

Matiazzo et al. [19] employed 3D CFD to investigate drag coefficients, coalescence, and breakdown models in the churn turbulent flow regime. Twelve configurations of coalescence and disintegration were examined in the investigation. The significance of utilizing the appropriate coalescence and breakage models was underscored by the results, as the breakdown model significantly influenced flow predictions more than the coalescence model. It was the Schiller and Naumann [20] model that most accurately predicted drag closure in comparison to experimental findings. The experimental results were consistent with the CFD simulations, which exhibited low gas velocity and gas holdup errors. The gas velocity predictions in the reactor centre were more precise than those at the walls, as the simulations overestimated the experimental measurements. Ertekin et al. [21] verified the CFD simulations of Fletcher et al. (2017) by adjusting the column radius and superficial gas velocity. Two-phase Euler-Euler models with a predetermined single bubble size were validated by Fletcher et al. [22]. The liquid phase was analysed using a typical k-ε turbulence approach. Ertekin et al. confirmed Fletcher's models, observing only a minor percentage discrepancy in holdup investigations.

Yan et al. [23] employed numerous drag models to investigate the hydrodynamics of BCR. The reactor was 660 cm tall and 30 cm wide, with 128 holes of 5mm diameter and a gas sparger located 20 cm from the base. The investigation contrasted electrical resistance tomography data with two- and three-dimensional computational fluid dynamics (CFD) models. In the cold-water air model of the bubble column, the radial gas holdup increased as the superficial gas velocity increased. Radial gas holdup was increased by an increase in internal pressure, particularly in the vicinity of the column centre. These tendencies were consistent with the experimental results and two and three CFD models. Adam and Tuwaechi [24] employed a two-phase CFD model with coarse and fine meshes, employing a Eulerian-Eulerian approach and a k-ε turbulence model to investigate gas holdup. Their simulated BCR was 19 cm in width and 96 cm in height. The model demonstrated that the volume fraction increased as the time step increased, with observations that were more detailed at 0.005 mesh resolutions. Additionally, they discovered that the gas pressure reached its maximum near the inlet and then decreased as it departed.

Euler-Euler simulation was employed by Pourtousi et al. [25] to investigate bubble column regimes. The SBC in their three-dimensional CFD model was 28.8 cm wide and 260 cm tall. Experimental and simulated data were compared to evaluate accuracy. In the bulk region, superficial gas velocities were predicted to range from 0.0025 to 0.015 m/s for a bubble diameter

of 3 mm. In a homogeneous domain, a single bubble diameter can be computationally efficient and effective. However, in a heterogeneous regime, a diversity of bubble sizes and an appropriate drag model may increase their accuracy. Homogeneous flows exhibit homogeneous bubble sizes and shapes with minimal interaction, whereas heterogeneous flows have bubbles that range from 0.05 mm to 50 mm, which affects reactor dynamics. Abdulrahman employed 2D CFD simulations to investigate the hydrodynamics of SBCR and DCHT [26-30]. The study examined the impact of liquid height, superficial gas velocity, and solid concentration on the volumetric heat transfer coefficient, temperature distributions, and SBCR gas holdup. 3D CFD was employed by Abdulrahman and Nassar [31-35] to investigate the hydrodynamics of oxygen reactors.

The objective of this investigation is to examine the hydrodynamics of the oxygen reactor in the Cu-Cl cycle, with a particular emphasis on the urgent need to address climate change and the potential of hydrogen as a sustainable energy carrier. Utilizing the ANSYS Fluent software, the investigation implements three-dimensional computational fluid dynamics (CFD) models. The results' accuracy and dependability are ensured by comparing the simulation findings with empirical data from previous experimental studies, which is how validation is achieved.

2. CFD Analysis
2.1. Governing Equations

A three-dimensional system is analysed in this work using computational fluid dynamics (CFD) simulations. The simulations feature a pressure-based solver, a Eulerian-Eulerian model, and a Eulerian sub-model. Table 1 outlines the mathematical equations employed in the computational fluid dynamics (CFD) investigation. The gas phase is the intended application of these equations. The equations for the slurry phase are not restated in order to be concise, as they are similar to the equations for the gas phase.

Table 1: Details of equations used in the 3D CFD simulations.

Description [reference]	Equation
Volume equation [36]	$V_g = \int_V \alpha_g \, dV$

Description [reference]	Equation
Continuity equation in 3D Polar coordinates (r, θ, y) [3]	$\nabla . V_g = \frac{\partial v_{r,g}}{\partial r} + \frac{v_{r,g}}{r} + \frac{1}{r}\frac{\partial v_{\theta,g}}{\partial \theta} + \frac{\partial v_{y,g}}{\partial y} = 0$
Momentum equation in 3D Polar coordinates [3]	$\rho_g \alpha_g (\frac{\partial v_r}{\partial t} + v_r \frac{\partial v_r}{\partial r} + \frac{v_\theta}{r}\frac{\partial v_r}{\partial \theta} + vy \frac{\partial v_r}{\partial y} - \frac{v_\theta^2}{r}) = -\alpha_g \frac{\partial P}{\partial r} + \alpha_g \frac{\mu_{g,eff}}{3}\frac{\partial(\nabla . V)}{\partial r} + \mu_{g,eff} \, \alpha_g [\frac{1}{r}\frac{\partial}{\partial r}(r\frac{\partial v_r}{\partial r}) + \frac{1}{r^2}\frac{\partial^2 v_r}{\partial \theta^2} + \frac{\partial^2 v_r}{\partial y^2} - \frac{v_r}{r^2} - \frac{2}{r^2}\frac{\partial v_\theta}{\partial \theta}] + \rho_g \alpha_g \, g_r + M_{i,g,r}$ $\rho_g \alpha_g (\frac{\partial v_\theta}{\partial t} + v_r \frac{\partial v_\theta}{\partial r} + \frac{v_\theta}{r}\frac{\partial v_\theta}{\partial \theta} + v_y \frac{\partial v_\theta}{\partial y} + \frac{v_r v_\theta}{r}) = -\alpha_g \frac{1}{r}\frac{\partial P}{\partial \theta} + \alpha_g \frac{\mu_{g,eff}}{3r}\frac{\partial(\nabla . V)}{\partial \theta} + \alpha_g \mu_{g,eff}[\frac{1}{r}\frac{\partial}{\partial r}(r\frac{\partial v_\theta}{\partial r}) + \frac{1}{r^2}\frac{\partial^2 v_\theta}{\partial \theta^2} + \frac{\partial^2 v_\theta}{\partial y^2} + \frac{2}{r^2}\frac{\partial v_r}{\partial \theta} - \frac{v_\theta}{r^2}] + \rho_g \alpha_g \, g_\theta + M_{i,g,\theta}$ $\rho_g \alpha_g (\frac{\partial v_y}{\partial t} + v_r \frac{\partial v_y}{\partial r} + \frac{v_\theta}{r}\frac{\partial v_y}{\partial \theta} + v_y \frac{\partial v_y}{\partial y}) = -\alpha_g \frac{\partial P}{\partial y} + \alpha_g \, \mu_{g,eff}[\frac{1}{r}\frac{\partial}{\partial r}(r\frac{\partial v_y}{\partial r}) + \frac{1}{r^2}\frac{\partial^2 v_y}{\partial \theta^2} + \frac{\partial^2 v_y}{\partial y^2}] + \rho_g \alpha_g g_y + M_{i,g,y}$
Energy equation in 3D Polar coordinates [3]	$\alpha_g \rho_g C (\frac{\partial T_g}{\partial t} + v_{r,g}\frac{\partial T_g}{\partial r} + \frac{v_{\theta,g}}{r}\frac{\partial T_g}{\partial \theta} + v_{y,g}\frac{\partial T_g}{\partial y}) = \bar{\bar{\tau}}_g : \nabla V_g + k_g (\frac{1}{r}\frac{\partial}{\partial r}(r\frac{\partial T_g}{\partial r}) + \frac{1}{r^2}\frac{\partial^2 Tg}{\partial \theta^2} + \frac{\partial^2 T_g}{\partial y^2}) + S_g + Q_{g,sl}$
Effective density	$\hat{\rho}_g = \alpha_g \, \rho_g$
Drag force [36]	$M_D = \frac{\rho_g f}{6 \, \tau_b} \, d_b \, A_i \, (\boldsymbol{V_g} - \boldsymbol{V_l})$
Interfacial area [36]	$A_i = \frac{6 \, \alpha_g \, (1 - \alpha_g)}{d_b}$
Schiller-Naumann drag equation [20]	$C_D = \begin{cases} \frac{24 \, (1 + 0.15 \, Re_b^{0.687})}{Re_b} & Re_b \leq 1000 \\ 0.44 & Re_b > 1000 \end{cases}$

The dimensions of the reactor in this study are determined in accordance with the Helium-Water bubble column reactor that Abdulrahman investigated [15-17]. Nevertheless, the material properties have been altered to align with the properties of Cupreous Chloride and oxygen. The O_2-CuCl system and the Helium-Water

(He-H_2O) systems exhibit similarities, as indicated by Abdulrahman's property comparison [24-25]. The superficial gas velocity of the O_2-CuCl system is precisely adjusted to align with the Reynolds number of the He-H_2O system in order to ensure consistency. The reactor employed in this investigation is cylindrical in shape, with a diameter of 21.6 cm and a height of 91.5 cm. A gas distributor of the sparger type, which has six arms, is employed to inject the gas into the bubble column reactor. The total number of holes is 72, as each arm is provided with 12 orifices, each of which has a diameter of 0.3 cm.

The Reynolds-Averaged Navier-Stokes (RANS) models, specifically the k-ε and k-ω models, are employed in this investigation. The most cost-effective methods for estimating complex turbulent flows have been shown to be these models. These models are capable of accurately simulating a wide range of turbulent flows and heat transfer processes. In contrast to the conventional k-ε model, the RNG k-ε model is chosen for its superior accuracy and reliability across a wider range of fluxes. This model is particularly well-suited for the simulation of turbulent flow that is associated with churn, which is the primary focus of this research. The dispersed turbulence model is the k-ε sub-model that was selected due to its ability to accurately represent the low concentrations of the gas phase and the distinct phase densities of the liquid and gas. In addition, this turbulence model is more cost-effective in terms of computational resources than the per-phase turbulence model. The standard wall function is a widely used model in industries because it can produce satisfactory results for a variety of flows that are bounded by walls. Typically, the wall boundary conditions are modelled using this function.

In this investigation, the 3D Bubble Column Reactor (BCR) is modelled using the ANSYS Fluent software. ANSYS Fluent is employed to establish the simulation's setup and boundary conditions. The Bubble Column Reactor (BCR) employs a hexahedron mesh, and mesh independence is utilized to determine the optimal mesh size that balances computational costs with satisfactory results. The gas holdup disparity is 3% when more refined meshes are employed, as the ultimate mesh is composed of 26,825 nodes and 24,396 elements (Fig. 1).

2.2. Boundary Conditions

The simulated BCR consists of three separate boundaries: the wall boundary conditions and the inlet and outlet boundary conditions. The boundary condition at the inlet is defined with a gas at a constant velocity and a volume fraction of 1. At the inlet of the sparger, the gas velocity is determined by dividing the volumetric flow rate of the gas at the inlet $\left(\dot{V}_{g,in}\right)$ by the entire cross-sectional area of the sparger (A).

$$v_g = \frac{\dot{V}_{g,in}}{A}$$

A superficial gas velocity U_{gs} is obtained by multiplying the gas velocity v_g by the gas volume fraction α_g.

$$U_{gs} = \alpha_g v_g$$

Since the volume percentage of the gas passing through the sparger equals 1, the superficial gas velocity at the inlet is equivalent to the gas velocity at the inlet. From above, the boundary conditions at the inlet will be:

At $y = 0, \alpha_g = 1$ and $U_{gs} = \alpha_g v_g = v_g = \frac{\dot{V}_{g,in}}{A}$

Due to the assumption of an incompressible gas phase and a relatively low pressure drop system, the pressure at the inlet is not provided. In order to achieve improved convergence results and prevent liquid entrainment with gas, the pressure boundary condition is implemented at the outlet of the column. In all cases, the pressure at the outlet is set to atmospheric pressure.

At $y = H, P = P_{atm}$

The walls are specified with a no-slip condition for the gas and liquid phases. Thus, for a reactor of radius R, the following boundary condition is applied at the wall:

At $r = R, v_{y,g} = 0$ and $v_{y,l} = 0$

To enhance understanding of hydrodynamics, the model did not incorporate any symmetry requirements. Given the challenging nature of approximating the effects of turbulence at the boundary of liquid, 5000 iterations were used to precisely determine the turbulent kinetic energy k and dissipation rate ε at the inlets and outlets.
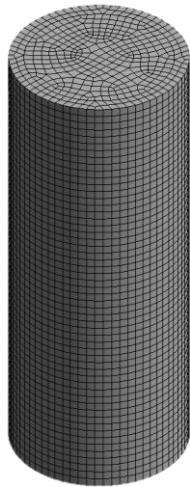
Fig. 1 BCR hexahedron mesh.

Fig. 2 Average gas holdup versus static liquid height and superficial gas velocity of CuCl-O₂.
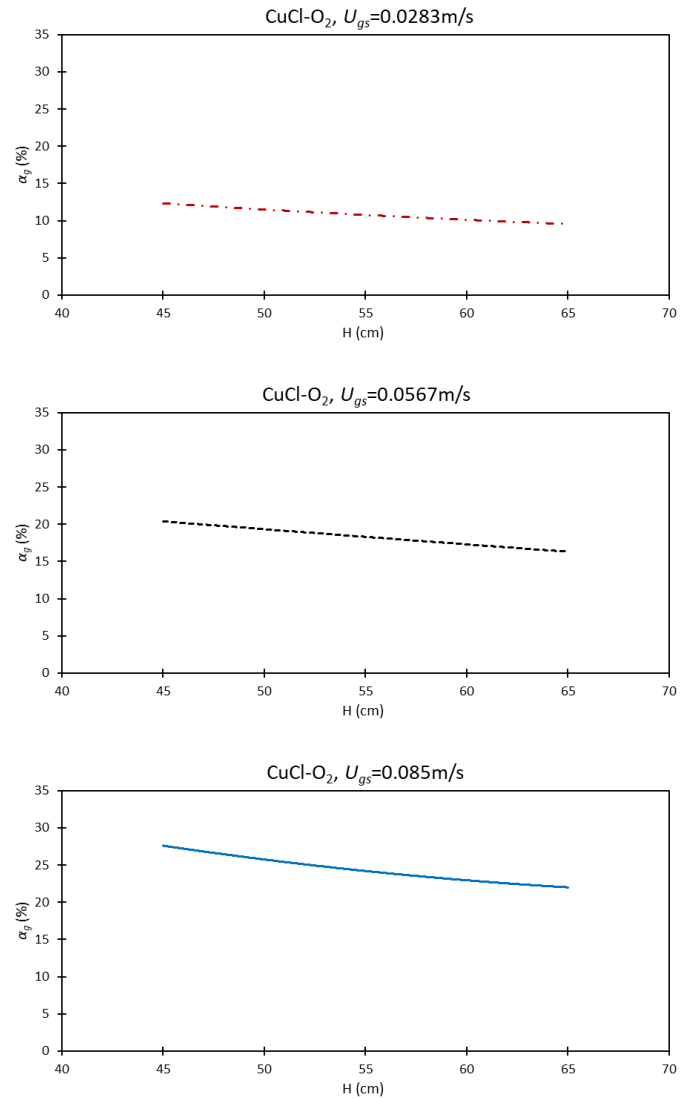

Fig. 3 Average gas holdup versus static liquid height of CuCl-O₂ at different superficial gas velocities.

3. Results

3. 1. Gas Holdup Versus Static Liquid Height

The three-dimensional curves of the gas holdup in relation to the superficial gas velocity (U_{gs}) and the static liquid height (H) are shown in Figure 2. The effects of varying H (45, 55, 65cm) on the gas holdup while changing U_{gs} for an O_2-CuCl system are illustrated in Figure 3. The contours of the cut sections of the BCR taken in the centre of the XY and ZY planes are shown in Figures 4-6. In order to facilitate a more comprehensive contour of α_g, additional cut sections are obtained at heights of 10, 20, and 30 cm from the reactor's base on the ZX plane. The gas holdup's behaviour is firmly three-dimensional, as evidenced by the contours, which clearly indicate that it is not symmetrical on the XY, ZY, and ZX planes. It has been noted that the value of α_g decreases as H increases. The gas holdup decreases by 20% when H is increased from 45 cm to 65 cm at a superficial gas velocity of 0.085 m/s.
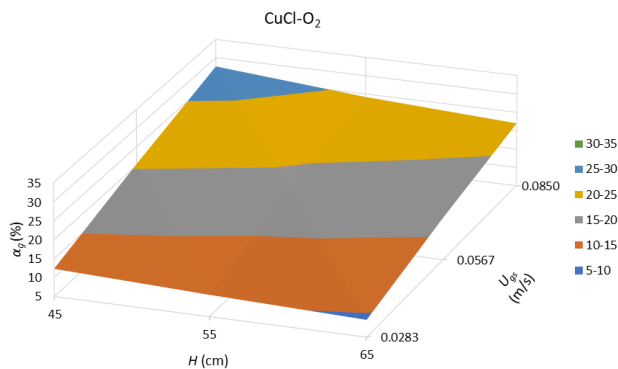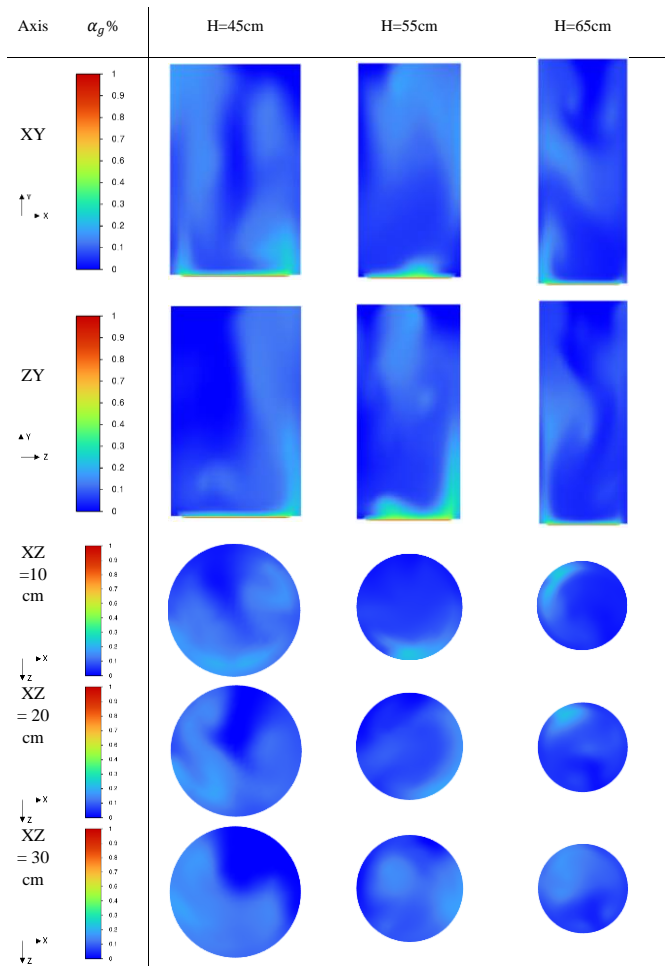
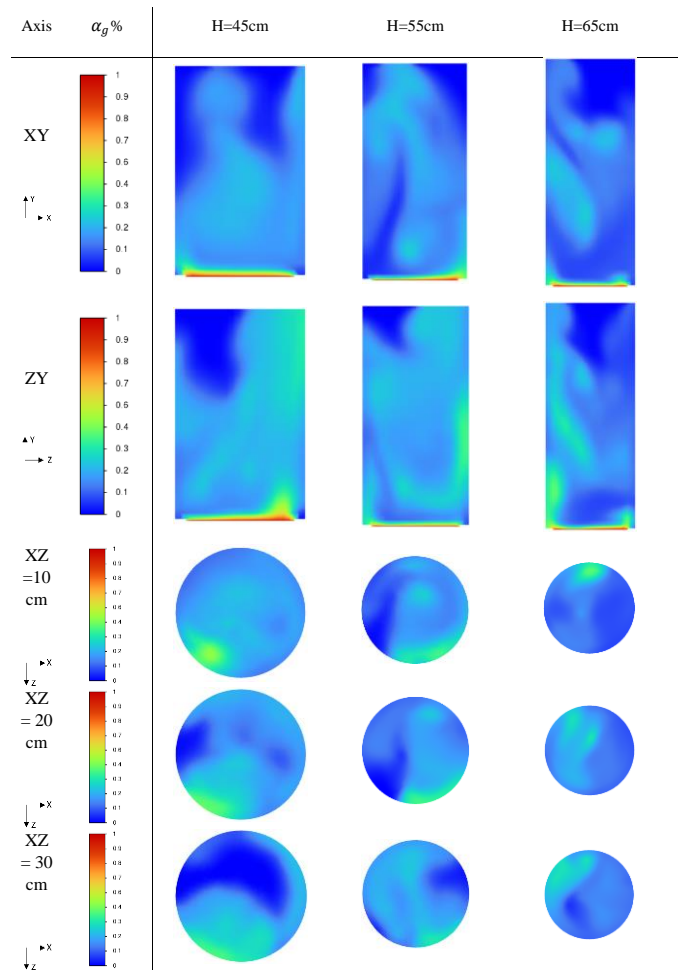Fig. 4 Oxygen-Cupreous Chloride gas holdup contours for $U_{gs} = 0.0283$ m/s.

Fig. 5 Oxygen-Cupreous Chloride gas holdup contours for $U_{gs} = 0.0567$ m/s.
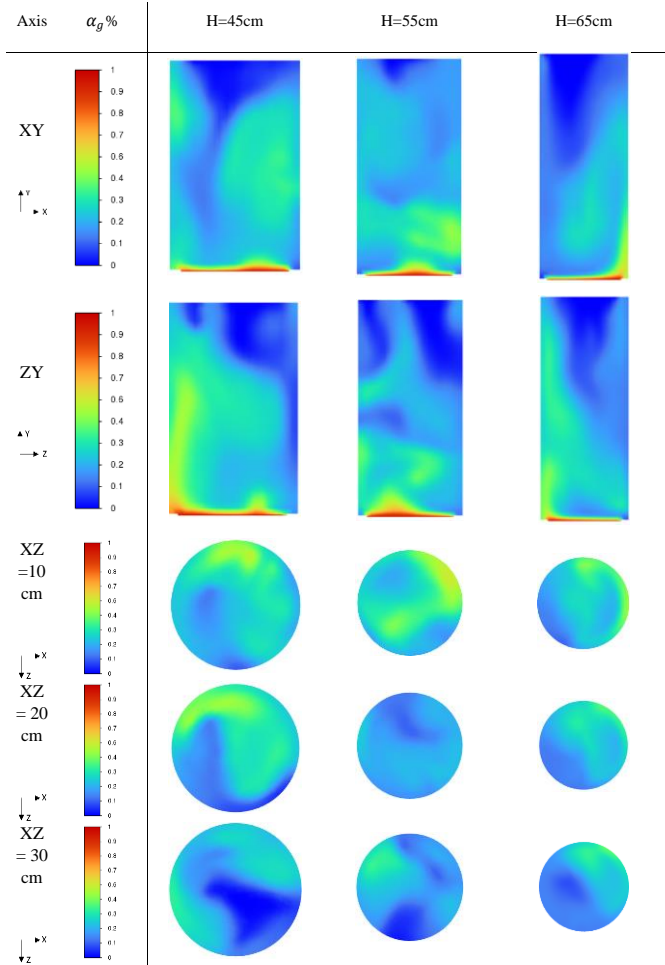
Fig. 6 Oxygen-Cupreous Chloride gas holdup contours for $U_{gs} = 0.085$ m/s.

3. 2. Comparative Analysis of 3D-CFD Models: Water-Helium Versus Copper Chloride-Oxygen Systems

Table 2 illustrates the dimensionless groups of hydrodynamics of the actual materials (CuCl and O_2) and the simulated materials (He and H_2O), as detailed in Abdulrahman's research [13-14]. The dimensionless groups' primary source of error is the density ratio of gas to liquid, with a magnitude of 11.311%. The corresponding percentage of errors resulting from the disparity between the actual and simulated materials, as well as the calculated gas holdup values, are presented in Table 3. 48.6% is the maximum percentage of inaccuracy, as the data obviously demonstrates. Additionally, it is clear that the gas holdup values in the actual materials are generally underestimated in comparison to those in the simulated materials. In order to replicate the effects of the simulated substances, the superficial gas velocities of the actual substances were

altered. Table 2 indicates that the cumulative effect of the percentage errors generated by each of the hydrodynamic dimensionless parameters is responsible for the elevated percentage error. Furthermore, this error is exacerbated by the complex three-dimensional multiphase system. The patterns and behaviours observed in the SBCR were accurately predicted by the 3D CuCl-O_2 simulation.

Table 2 Error analysis of dimensionless groups in actual vs. experimental materials studies [13-14].

Dimensionless Group	Actual Material	Experimental Materials	Error%
$\dfrac{\rho_g}{\rho_l}$	0.000121	0.000135	11.311
$\dfrac{\mu_g}{\mu_l}$	0.021756	0.023	6.908
$\dfrac{Re_l^2}{We_l}$	76473868 (D_R=1m)	76085070 (D_R=1m)	0.508

Table 3 Error Analysis of Superficial Gas Velocity and Gas Holdup in H_2O-He and CuCl-O_2 Systems.

Water-Helium		Cupreous Chloride-Oxygen		Percent Error
U_{gs} (m/s)	α_g(%)	U_{gs} (m/s)	α_g(%)	(%)
H=45 cm				
0.05	16.0	0.0283	12.3	29.9
0.1	24.4	0.0576	20.4	19.6
0.15	31.3	0.085	27.6	13.3
H=55 cm				
0.05	15.0	0.0283	10.8	39.4
0.1	22.7	0.0576	18.3	24.0
0.15	28.0	0.085	24.2	15.7
H=65 cm				
0.05	14.2	0.0283	9.5	48.6
0.1	21.7	0.0576	16.3	33.1
0.15	26.5	0.085	22.0	20.5

In Fig. 4, it is evident that the gas holdup's behaviour in relation to the static liquid height is consistent across both the H_2-H_2O and O_2-CuCl systems. Specifically, the gas holdup decreases as the static liquid height increases.

(a) H₂O- He

Ugs=0.05m/s   Ugs=0.1m/s
Ugs=0.15m/s

(b) CuCl-O₂

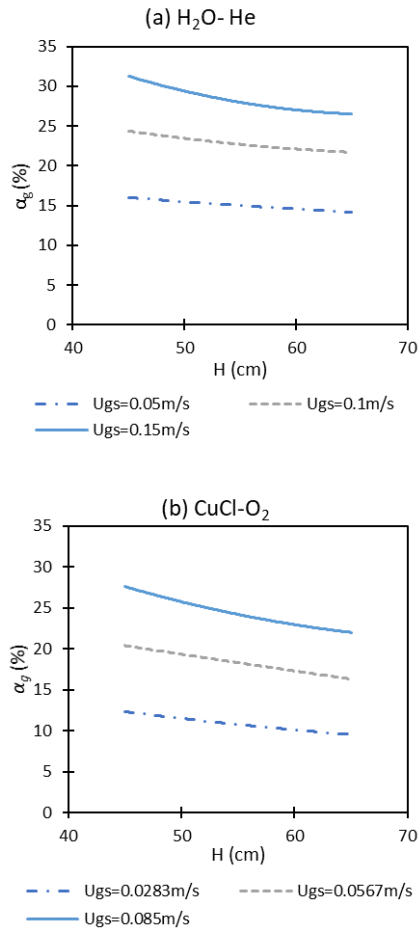Ugs=0.0283m/s   Ugs=0.0567m/s
Ugs=0.085m/s

Fig. 4 Comparison of Average Gas Holdup Versus Static Liquid Height for (a) Water-Helium system (b) Cupreous Chloride-Oxygen system.

4. Conclusions

The purpose of this investigation is to verify the efficacy of substitute materials, particularly liquid water and helium gas, as replacements for the actual materials, namely molten CuCl and oxygen gas, in the oxygen bubble column reactor that is employed in the thermochemical copper-chlorine (Cu-Cl) cycle of hydrogen production. The validation procedure entails the use of ANSYS Fluent software to conduct 3D computational fluid dynamics (CFD) simulations. The simulations are particularly designed to investigate various static liquid heights in the CuCl-O₂ system. The analysis confirms that the gas holdup patterns are consistent across both three-dimensional computational fluid dynamics (CFD) models. Furthermore, the gas holdup in the 3D CFD results of the O₂-CuCl system

is consistently lower than that in the 3D CFD findings of the He-H₂O system.

List of Symbols

A_i	Interfacial area concentration
C	Specific heat
C_D	Drag coefficient
d_b	Bubble diameter
g	Gravitational acceleration
H	Height
Mi	Total interfacial forces between the phases
P	Phase pressure
$Q_{g,l}$	Intensity of heat exchange
Re	Reynolds number
T	Temperature
v	Velocity field
V_g	Volumes of gas
V_l	Volumes of liquid
U_{gs}	Superficial gas velocity
α_g	Gas holdup
μ_{eff}	Effective viscosity
μ_g	Dynamic viscosity gas
μ_l	Dynamic viscosity liquid
ρ_g	Density, gas
ρ_l	Density, liquid
$\bar{\bar{\tau}}: \nabla V$	Viscous stress tensor

References

[1] Lewis, M. A., M. Serban, and J. K. Basco. "Generating hydrogen using a low temperature thermochemical cycle." In *Proceedings of the ANS/ENS 2003 Global International Conference on Nuclear Technology, New Orleans*. 2003.

[2] Serban, M., M. A. Lewis, and J. K. Basco. "Kinetic study of the hydrogen and oxygen production reactions in the copper-chloride thermochemical cycle." *AIChE 2004 spring national meeting, New Orleans, LA*. 2004.

[3] Abdulrahman, Mohammed W. "Analysis of the thermal hydraulics of a multiphase oxygen production reactor in the Cu-Cl cycle." Diss. University of Ontario Institute of Technology (Canada), 2016.

[4] Abdulrahman, Mohammed Wassef. "Direct contact heat transfer in the thermolysis reactor of hydrogen production Cu—Cl cycle." U.S. Patent No. 10,059,586. 28 Aug. 2018.

[5] Abdulrahman, Mohammed W. "Scale-up Analysis of Three-Phase Oxygen Reactor in the Cu-Cl

Thermochemical Cycle of Hydrogen Production." *Proceedings of EIC Climate Change Technology Conference (CCTC2013)*. 2013.

[6] Abdulrahman, M. W., Wang, Z., Naterer, G. F., & Agelin-Chaab, M. "Thermohydraulics of a thermolysis reactor and heat exchangers in the Cu-Cl cycle of nuclear hydrogen production." in *Proceedings of the 5th World Hydrogen Technologies Convention,* 2013.

[7] Abdulrahman, Mohammed W. "Similitude for Thermal Scale-up of a Multiphase Thermolysis Reactor in the Cu-Cl Cycle of a Hydrogen Production." *International Journal of Energy and Power Engineering,* vol. 10, no. 5, pp. 664-670, 2016.

[8] Abdulrahman, Mohammed W. "Heat Transfer Analysis of a Multiphase Oxygen Reactor Heated by a Helical Tube in the Cu-Cl Cycle of a Hydrogen Production." *International Journal of Mechanical and Mechatronics Engineering,* vol. 10, no. 6, pp. 1122-1127, 2016.

[9] Abdulrahman, Mohammed W. "Heat transfer in a tubular reforming catalyst bed: Analytical modelling." *proceedings of the 6th International Conference of Fluid Flow, Heat and Mass Transfer*. 2019.

[10] Abdulrahman, Mohammed W. "Exact Analytical Solution for Two-Dimensional Heat Transfer Equation Through a Packed Bed Reactor." *Proceedings of the 7th World Congress on Mechanical, Chemical, and Material Engineering (MCM'20)*. 2020.

[11] Abdulrahman, Mohammed W. "Heat Transfer Analysis of the Spiral Baffled Jacketed Multiphase Oxygen Reactor in the Hydrogen Production Cu-Cl Cycle." In *Proceedings of the 9th International Conference on Fluid Flow, Heat and Mass Transfer (FFHMT'22)*, 2022.

[12] Abdulrahman, Mohammed W. " Thermal Efficiency in Hydrogen Production: Analyzing Spiral Baffled Jacketed Reactors in the Cu-Cl Cycle." *Journal of Engineering Research,* vol. 4, no. 10, 2024.

[13] Abdulrahman, Mohammed W. "Simulation of Materials Used in the Multiphase Oxygen Reactor of Hydrogen Production Cu-Cl Cycle." *Proceedings of the 6 the International Conference of Fluid Flow, Heat and Mass Transfer (FFHMT'19)*. 2019.

[14] Abdulrahman, Mohammed Wassef. "Material substitution of cuprous chloride molten salt and

oxygen gas in the thermolysis reactor of hydrogen production Cu—Cl cycle." U.S. Patent No. 10,526,201. 7 Jan. 2020.

[15] Abdulrahman, M. W. "Experimental studies of direct contact heat transfer in a slurry bubble column at high gas temperature of a helium–water–alumina system." *Applied Thermal Engineering,* vol. 91, pp. 515-524, 2015.

[16] Abdulrahman, M. W. "Experimental studies of gas holdup in a slurry bubble column at high gas temperature of a helium− water− alumina system." *Chemical Engineering Research and Design*, vol. 109, pp. 486-494, 2016.

[17] Abdulrahman, M. W. "Experimental studies of the transition velocity in a slurry bubble column at high gas temperature of a helium–water–alumina system." *Experimental Thermal and Fluid Science,* vol. 74, pp. 404-410, 2016.

[18] Abdulrahman, Mohammed W., and Nibras Nassar. "Eulerian Approach to CFD Analysis of a Bubble Column Reactor–A." In *Proceedings of the 8th World Congress on Mechanical, Chemical, and Material Engineering (MCM'22)*, 2022.

[19] Matiazzo, T., Decker, R.K., Bastos, J.C.S.C., Silva, M.K. and Meier, H. "Investigation of Breakup and Coalescence Models for Churn-Turbulent Gas-Liquid Bubble Columns." *Journal of Applied Fluid Mechanics* vol. 13, no. 2, pp. 737-751, 2020.

[20] Schiller, L. (1933). A drag coefficient correlation. *Zeit. Ver. Deutsch. Ing.*, vol. 77, pp.318-320, 1933.

[21] Ertekin, E., Kavanagh, J.M., Fletcher, D.F. and McClure, D.D. "Validation studies to assist in the development of scale and system independent CFD models for industrial bubble columns." *Chemical Engineering Research and Design*, vol. 171, pp. 1-12, 2021.

[22] Fletcher, David F., McClure, D.D, Kavanagh, J.M., Barton, G.W. "CFD Simulation of Industrial Bubble Columns: Numerical Challenges and Model Validation Successes." *Applied Mathematical Modelling*, vol. 44, pp. 25–42, 2017.

[23] Yan, P., Jin, H., He, G., Guo, X., Ma, L., Yang, S. and Zhang, R. "CFD simulation of hydrodynamics in a high-pressure bubble column using three optimized drag models of bubble swarm." *Chemical Engineering Science*, vol. 199, pp. 137-155, 2019.

[24] Adam, Salman, and Kalthoum Tuwaechi. "Hydraulic Simulation of Bubble Flow in

Bubble Column Reactor." *Journal of Complex Flow* vol.1, no.2, Dec. 2019.

[25] Pourtousi, M., P. Ganesan, and J. N. Sahu. "Effect of bubble diameter size on prediction of flow pattern in Euler–Euler simulation of homogeneous bubble column regime." *Measurement*, vol. 76, pp. 255-270, 2015.

[26] Abdulrahman, M.W. "CFD Simulations of Direct Contact Volumetric Heat Transfer Coefficient in a Slurry Bubble Column at a High Gas Temperature of a Helium–Water–Alumina System." *Applied Thermal Engineering*, vol. 99, pp. 224–234, 2016.

[27] Abdulrahman, Mohammed W. "CFD Analysis of Temperature Distributions in a Slurry Bubble Column with Direct Contact Heat Transfer." In *Proceedings of the 3rd International Conference on Fluid Flow, Heat and Mass Transfer (FFHMT'16)*. 2016.

[28] Abdulrahman, Mohammed W. "CFD Simulations of Gas Holdup in a Bubble Column at High Gas Temperature of a Helium-Water System." In *Proceedings of the 7th World Congress on Mechanical, Chemical, and Material Engineering (MCM'20),* 2020.

[29] Abdulrahman, Mohammed W. "Effect of Solid Particles on Gas Holdup in a Slurry Bubble Column." In *Proceedings of the 6th World Congress on Mechanical, Chemical, and Material Engineering*, 2020.

[30] Abdulrahman, Mohammed W. "Temperature profiles of a direct contact heat transfer in a slurry bubble column." *Chemical Engineering Research and Design,* vol. 182, pp. 183-193, 2022.

[31] Abdulrahman, Mohammed W., and N. Nassar. " Three Dimensional CFD Analyses for the Effect of Solid Concentration on Gas Holdup in a Slurry Bubble Column." *Proceedings of the 9th World Congress on Mechanical, Chemical, and Material Engineering (MCM'23)*. 2023.

[32] Abdulrahman, Mohammed W., and N. Nassar. " A Three-Dimensional CFD Analyses for the Gas Holdup in a Bubble Column Reactor." *Proceedings of the 9th World Congress on Mechanical, Chemical, and Material Engineering (MCM'23)*. 2023.

[33] Abdulrahman, Mohammed W., and N. Nassar. " Effect of Static Liquid Height on Gas Holdup of a Bubble Column Reactor." *Proceedings of the 9th World Congress on Mechanical, Chemical, and Material Engineering (MCM'23)*. 2023.

[34] Abdulrahman, M. W., & Nassar, N. "Hydrodynamic Analysis of Oxygen and Molten CuCl in the Cu-Cl Cycle Using a 3D CFD Model for Hydrogen Production" In *Proceedings of the 10th World Congress on Mechanical, Chemical, and Material Engineering (MCM'24)*, 2024.

[35] Abdulrahman, M. W., & Nassar, N. "Impact of Static Liquid Height on Hydrodynamics of the Thermolysis Reactor in the Cu-Cl Cycle for Hydrogen Production" In *Proceedings of the 10th World Congress on Mechanical, Chemical, and Material Engineering (MCM'24)*, 2024.

[36] ANSYS Inc. "ANSYS FLUENT Theory Guide." ANSYS FLUENT Theory Guide, Version 14.5, 2012.